

Lawrence Berkeley National Laboratory

Lawrence Berkeley National Laboratory

Title

Interstitial incorporation of plutonium into a low-dimensional potassium borate

Permalink

<https://escholarship.org/uc/item/5q8968gj>

Author

Wang, Shuao

Publication Date

2014-04-21

DOI

10.1021/es2028247

Peer reviewed

Interstitial Incorporation of Plutonium into a Low-Dimensional Potassium Borate

Shuao Wang,[†] Juan Diwu,[†] Antonio Simonetti,[†] Corwin H. Booth,[‡] Thomas E. Albrecht-Schmitt^{†}*

Department of Civil Engineering and Geological Sciences and Department of Chemistry and Biochemistry, University of Notre Dame, Notre Dame, IN 46556 and Chemical Sciences Division, Lawrence Berkeley National Laboratory, Berkeley, CA 94720

RECEIVED DATE ()

*Corresponding author email: talbrec1@nd.edu; phone: (574) 631-1872; fax: (574) 631-9236.

[†]University of Notre Dame, [‡]Lawrence Berkeley National Laboratory

Abstract The molten boric acid flux reaction of PuBr_3 with KBO_2 at 200 °C results in the formation of large light-yellow crystals of $\text{K}[\text{B}_5\text{O}_7(\text{OH})_2]\cdot\text{H}_2\text{O}:\text{Pu}^{4+}$ that are uniformly doped with plutonium. Single crystal X-ray diffraction experiments on the Pu-doped $\text{K}[\text{B}_5\text{O}_7(\text{OH})_2]\cdot\text{H}_2\text{O}$ demonstrates two features: (1) $\text{K}[\text{B}_5\text{O}_7(\text{OH})_2]\cdot\text{H}_2\text{O}:\text{Pu}^{4+}$ adopts a one-dimensional borate chain structure with large void spaces between the chains; (2) The doping plutonium atoms do not reside on the potassium sites. The latter are not fully occupied (3.2% defects). Both laser-ablation inductively coupled plasma mass spectrometry (LA-ICP-MS) and energy dispersive spectrometer (EDS) analyses indicate that plutonium atoms are uniformly distributed in crystals of $\text{K}[\text{B}_5\text{O}_7(\text{OH})_2]\cdot\text{H}_2\text{O}$ with an atomic K:Pu ratio of approximately 65:1 measured by LA-ICP-MS. UV-vis-NIR spectra taken from both freshly-made and one-day old crystals show that the plutonium present within the crystals is predominantly characterized by an oxidation state of IV. A small amount of Pu(III) is also present initially, but slowly oxidized to Pu(IV) via interaction with oxygen in the air. X-ray absorption near-edge structure (XANES) and extended X-ray absorption fine structure (EXAFS) spectroscopic measurements confirm that plutonium is mainly present as a form

similar to PuO_2 in the void spaces between the borate chains. $\text{K}[\text{B}_5\text{O}_7(\text{OH})_2]\cdot\text{H}_2\text{O}:\text{Pu}^{4+}$ provides a novel mechanism for incorporating heavy metal contaminants, including actinides, into natural materials.

Keywords: Interstitial incorporation, plutonium uptake, borate minerals, WIPP

Introduction

Nuclear weapon testing and plutonium production during the cold war, and recent events such as the catastrophe at the *Fukushima Daiichi* nuclear plant in Japan, resulted in the contamination of large areas of oceans, ground-water, soils, and sediments by actinides, such as uranium and plutonium, along with their fission and decay products. Thus, possible migration of actinides within contaminated sites becomes an important environmental concern (1-3). Generally, the incorporation of actinides into natural materials retards their migrations in the environment. Knowledge of the incorporation mechanisms of actinides into different types of natural materials is therefore required both for predicting the migration of radionuclides at the repositories and at contaminated sites, and for designing/manufacturing of suitable radioactive waste forms (4-6).

During the last two decades, significant efforts have been made to better understand the incorporation of early actinide elements (namely Th, U, Np, and Pu) into a variety of mineral phases, such as calcite (7-15), zircon (4,16-17), monazite (4,17-18), zirconolite (4,18-22), perovskite (4,22), garnet (4), pyrochlore (4,23-25), brucite (26), and several other systems (27-30). Particularly for transuranium elements (Np and Pu), it was determined that these can also be incorporated into a series of uranium- or thorium- based minerals such as brannerite (4), ianthinite (31), schoepite, becquerelite, compregnacite, and boltwoodite (32) or even synthetic phases such as $\text{Th}_{2-x/2}\text{An}_{x/2}^{\text{IV}}(\text{PO}_4)_2(\text{HPO}_4)\cdot\text{H}_2\text{O}$ ($\text{An} = \text{U}, \text{Np}, \text{Pu}$) (33), ThSiO_4 (34), and $\text{Ba}_3(\text{UO}_2)_2(\text{HPO}_4)_2(\text{PO}_4)_2$ (35). The majority of studies focused on examining incorporation mechanisms indicate the presence of a suitable crystallographic site in the

lattice for actinide units to reside in the incorporated materials; i.e. the actinide units substitute into lattice sites that are occupied by other cations that have similar crystal chemistry. This commonly occurring mechanism is termed “substitutional incorporation.” For example, numerous studies indicate that trace amounts of uranium, present as both U(VI) and U(IV), can be incorporated into natural calcite (7-14). U(IV) was found to have a stable location on the sites of divalent calcium (7), while U(VI) occupies mainly calcium sites along with other possible defects or disordered sites (8-9). For cases of plutonium incorporation, Pu(IV) substitutes into calcium sites in zirconolites (19), and Pu(III) can enter the structure of monazite in the position of La(III) (18). Furthermore, Pu(VI) can readily occur in many structures containing U(VI) by substituting onto the U(VI) sites (31-32). In light of all these observations, one could conclude that the high level incorporation of actinides requires suitable crystallographic sites in the lattice of materials.

We have recently undertaken a study involving the preparation, structural elucidation, and physico-chemical property measurements of actinide borates (36-47). In an attempt to prepare a plutonium(IV) borate compound, a potassium borate that is doped with Pu(IV) was discovered. This compound, with a formula of $\text{K}[\text{B}_5\text{O}_7(\text{OH})_2] \cdot \text{H}_2\text{O}$, contains no suitable lattice sites for the plutonium substitution. However, it was determined that high levels of Pu(IV) are capable of entering the structure of $\text{K}[\text{B}_5\text{O}_7(\text{OH})_2] \cdot \text{H}_2\text{O}$ with an atomic ratio K:Pu around 65:1, as measured by LA-ICP-MS. We have used both single crystal X-ray diffraction, X-ray absorption near-edge structure (XANES), and extended X-ray absorption fine structure (EXAFS) to demonstrate that Pu(IV) can enter the void spaces between the neighboring borate chains while removing some lattice potassium to maintain charge-balance. Interstitial incorporation suggests a novel approach for understanding how actinides can enter natural materials, although the interstitial incorporation mechanism was found in a few other, non-actinide-bearing systems (48-50). In this paper, we will describe both the synthesis and characterizations of $\text{K}[\text{B}_5\text{O}_7(\text{OH})_2] \cdot \text{H}_2\text{O}:\text{Pu}^{4+}$, and demonstrate this novel incorporation mechanism that does not involve lattice substitution.

Experimental section

Syntheses. Specialized facilities and procedures are needed for this work. All free-flowing solids were handled within negative-pressure gloveboxes, and products were examined when coated with either water or Krytox oil and water. $^{242}\text{PuO}_2$ (99.98% isotopic purity, Oak Ridge National Laboratory, $t_{1/2} = 3.76 \times 10^5$ y) was used as received. While the plutonium is of very high isotopic purity, there are trace amounts of ^{238}Pu , ^{240}Pu , ^{241}Pu , ^{244}Pu , and ^{241}Am . The majority of the radioactivity comes from the ^{241}Pu even though it represents only 0.008% of the plutonium. *^{242}Pu still represents a serious health risk owing to its α and γ emission.* This isotope was selected because of its long half-life, which increased the longevity of the crystals. A 0.365 M stock solution of $^{242}\text{Pu(VI)}$ nitrate was prepared by first digesting PuO_2 in 8 M HNO_3 for 3 days at 200 °C in an autoclave. The solution was then reduced to a moist residue and redissolved in water. This solution was then ozonated for approximately 5 hours to ensure complete oxidation of the plutonium to +6.

An aliquot containing 5 mg of plutonium(VI) was taken from the above stock solution and reduced to a residue. 50 μL of concentrated HBr was added to this residue resulting in the immediate formation of bromine gas and a red solution (the red color is from the dissolved bromine which masks the color of Pu(III)). The red solution was reduced to a purple-black residue at 130 °C. The residue was redissolved in 30 μL of argon-sparged water producing a navy blue/purple solution characteristic of Pu(III) . A droplet of Pu(III) was then transferred to a PTFE autoclave liner. A large excess of boric acid (47 mg) and KBO_2 (7.8 mg) was then added directly to the droplet containing Pu(III) . The mixture was then sealed in an autoclave and heated at 200 °C for three days followed by slow cooling to room temperature over a period of two days. The autoclave was then opened and boiling water was added to dissolve the excess boric acid. The wash solution was almost colorless which indicates that an insignificant amount of Pu was released upon washing. Plutonium in solution was noted detected by UV-vis spectroscopy. Yellow crystals of $\text{K}[\text{B}_5\text{O}_7(\text{OH})_2] \cdot \text{H}_2\text{O} : \text{Pu}^{4+}$ with a tablet habit were then isolated as the pure product.

Crystallographic studies. A crystal of $\text{K}[\text{B}_5\text{O}_7(\text{OH})_2]\cdot\text{H}_2\text{O}:\text{Pu}^{4+}$ was mounted on a CryoLoop with Krytox oil and optically aligned on a Bruker APEXII Quazar X-ray diffractometer using a digital camera. Initial intensity measurements were performed using a $\text{I}\mu\text{S}$ X-ray source, a 30 W microfocused sealed tube ($\text{MoK}\alpha$, $\lambda = 0.71073 \text{ \AA}$) with high-brilliance and high-performance focusing Quazar multilayer optics. Standard APEXII software was used for determination of the unit cells and data collection control. The intensities of reflections of a sphere were collected by a combination of four sets of exposures. Each set had a different φ angle for the crystal and each exposure covered a range of 0.5° in ω . A total of 1464 frames were collected with an exposure time per frame of 30 s. SAINT software was used for data integration including Lorentz and polarization corrections. Semiempirical absorption corrections were applied using the program SCALE (SADABS) (51).

The crystal structure of $\text{K}[\text{B}_5\text{O}_7(\text{OH})_2]\cdot\text{H}_2\text{O}:\text{Pu}^{4+}$ was solved by direct methods. All atoms were refined anisotropically. The site occupancy factor refinement on the potassium sites showed that the sites are not fully occupied with an approximate 3.2% defect. Also, the substitutional disorder refinement on the potassium sites based on both K and Pu atoms failed to provide a reasonable occupancy, indicating the doping Pu atoms do not occupy K sites. However, it was still difficult to locate the doping Pu atoms in the final difference Fourier map, which indicates Pu atoms are highly disordered within the void space between the borate chains.

Laser-ablation inductively coupled plasma mass spectrometer (LA-ICP-MS) analysis. Laser ablation analysis of nine different crystals of $\text{K}[\text{B}_5\text{O}_7(\text{OH})_2]\cdot\text{H}_2\text{O}:\text{Pu}^{4+}$ were conducted using a ThermoFinnigan high resolution magnetic sector Element2 ICP-MS instrument coupled to a UP213 Nd:YAG laser ablation system (New Wave Research). Selected crystals were fixed on 1-inch round glass slides with double-sided tape. Individual analyses consisted of 60 seconds measurement of background ion signals followed by a 60 seconds interval of measurement of ion signals (^{11}B , ^{39}K , ^{242}Pu) subsequent the start of lasering. Each analysis represents a total of 93 scans (93 runs x 1 pass) with a sample (dwell) time of 0.01 second with 20 samples per ion signal peak. Analyses were

conducted in medium mass resolution mode (Resolution = Mass/Peak Width $\sim 4,000$) in order to eliminate possible spectral interferences. The ablated particles were transported from the ablation cell to the ICP-MS instrument using He carrier gas at a flow rate of 0.7 L/min. Crystals were ablated using a range of spot sizes between 40 and 55 μm , repetition rate of 2 Hz and 70% power output corresponding to an energy density of 12-15 J/cm^2 . Using these ablation conditions, the depth of penetration of the laser is between 5 and 15 microns (52-53).

Scanning electron microscopy and energy dispersive spectrometer (SEM/EDS) analysis.

SEM/EDS images and data were collected using a LEO EVO 50 with an Oxford INCA Energy Dispersive Spectrometer. The energy of the electron beam was set at 29.02 kV, and spectrum acquisition time was 120 seconds. All of the data were calibrated with standards and all EDS results are provided in the supporting information. Plutonium in the $\text{K}[\text{B}_5\text{O}_7(\text{OH})_2]\cdot\text{H}_2\text{O}:\text{Pu}^{4+}$ was easily identified in the energy dispersive spectrum and an atomic ratio K:Pu is given as 24.4:1 based on the average statistics for ten parallel measurements (Supporting Information).

UV-vis-NIR absorption spectroscopy. UV-vis-NIR data were acquired from both freshly-made and one day old crystals of $\text{K}[\text{B}_5\text{O}_7(\text{OH})_2]\cdot\text{H}_2\text{O}:\text{Pu}^{4+}$ using a Craic Technologies microspectrophotometer. Crystals were placed on quartz slides under Krytox oil, and the data were collected from 500 to 1400 nm. The exposure time was optimized automatically by the Craic software.

X-ray absorption spectroscopy. A sample of crystalline $\text{K}[\text{B}_5\text{O}_7(\text{OH})_2]\cdot\text{H}_2\text{O}:\text{Pu}^{4+}$ was measured at the Pu L_{III} edge on beamline 11-2 at the Stanford Synchrotron Radiation Lightsource (SSRL) using a Si(220) double monochromator ($\phi = 0^\circ$) detuned by 50% to avoid unwanted harmonics. Data were collected in fluorescence mode using a multi-element Ge detector and corrected for dead time. The data were also corrected for self-absorption (54) assuming 5% of the K atoms are replaced by Pu. The EXAFS data were reduced and fit in r -space (55) using standard procedures (56) using the RSXAP analysis suite (<http://lise.lbl.gov/RSXAP>). The XANES data are shown in Figure 5 and both the EXAFS data and fit are shown in Figure 6. EXAFS fits utilize scattering amplitudes and phases

calculated with the FEFF8.1 code (A.L. Ankudinov, B. Ravel, J.J. Rehr, and S.D. Conradson, Real Space Multiple Scattering Calculation of XANES, Phys. Rev. B 58, 7565-7576 (1998).) based on a PuO_2 fluorite structure.

Results and discussion

Syntheses. The pure phase of $\text{K}[\text{B}_5\text{O}_7(\text{OH})_2]\cdot\text{H}_2\text{O}:\text{Pu}^{4+}$ can be synthesized by the molten boric acid flux reaction of PuBr_3 with KBO_2 at 200 °C. Apparently, Pu(III) was slowly oxidized to Pu(IV) by O_2 in the atmosphere during the reaction. We found that a similar reaction in the absence of KBO_2 in the starting materials will result in the formation of a Pu(IV) borate. Thus, the presence of KBO_2 will kinetically eliminate the formation of plutonium(IV) borates. $\text{K}[\text{B}_5\text{O}_7(\text{OH})_2]\cdot\text{H}_2\text{O}:\text{Pu}^{4+}$ forms large yellow crystals with a tablet habit and are shown in Figure 1. The crystals can be cut, and the interior shows the same color as the surface, which excludes the case of surface absorption of Pu(IV) on the crystals of $\text{K}[\text{B}_5\text{O}_7(\text{OH})_2]\cdot\text{H}_2\text{O}$. Given that pure, non-doped $\text{K}[\text{B}_5\text{O}_7(\text{OH})_2]\cdot\text{H}_2\text{O}$ crystals are expected to be colorless, the yellow coloration indicates high levels of plutonium incorporation.

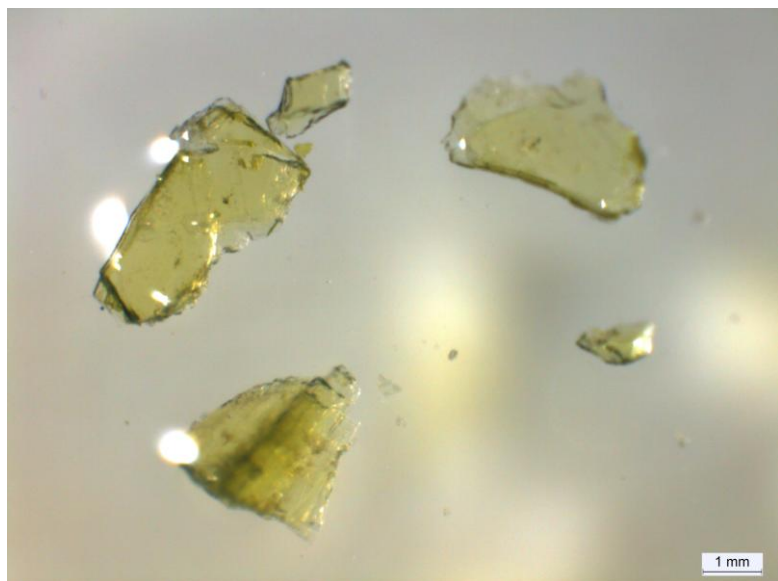


Figure 1. Photo of crystals of $\text{K}[\text{B}_5\text{O}_7(\text{OH})_2]\cdot\text{H}_2\text{O}:\text{Pu}^{4+}$.

Crystallographic studies. The synthesis and crystal structure of $\text{K}[\text{B}_5\text{O}_7(\text{OH})_2]\cdot\text{H}_2\text{O}$ was recently reported by Zhang et al. (57). The structure of $\text{K}[\text{B}_5\text{O}_7(\text{OH})_2]\cdot\text{H}_2\text{O}$ contains a series of double helical one-dimensional borate chains shown in Figure 2a. The potassium atoms are sitting in the void space within the double helical borate chains. There are larger void spaces present between the neighboring double chains (Figure 2b). The vertical distance for these void spaces along a axis is approximately 3.9 Å, which is compatible for trapping the eight-coordinated $\text{Pu}(\text{IV})\text{O}_8$ cubic polyhedra (Figure 2b). It should be noted that although $\text{K}[\text{B}_5\text{O}_7(\text{OH})_2]\cdot\text{H}_2\text{O}$ does not have an exact natural mineral analogue and can only be synthesized in the lab, the structure of larderellite, with the formula of $\text{NH}_4[\text{B}_5\text{O}_7(\text{OH})_2]\cdot\text{H}_2\text{O}$, is isotypic with $\text{K}[\text{B}_5\text{O}_7(\text{OH})_2]\cdot\text{H}_2\text{O}$ (Table 1) (58). By incorporating $\text{Pu}(\text{IV})$, the unit cell parameters for $\text{K}[\text{B}_5\text{O}_7(\text{OH})_2]\cdot\text{H}_2\text{O}:\text{Pu}^{4+}$ are slightly smaller than those for $\text{K}[\text{B}_5\text{O}_7(\text{OH})_2]\cdot\text{H}_2\text{O}$ reported by Yang et al. (Table 1). An approximate 3.2% defect was shown on K1 sites based on the site occupancy factor refinement. More importantly, the substitutional disorder refinement on K1 sites based on both K and Pu atoms fails to give a reasonable second free variable for occupancy determination. Together, these facts indicate that the doping Pu atoms are not occupying the K sites. This conclusion is reasonable from the point of view that there are large differences between $\text{Pu}(\text{IV})$ and K^+ in both coordination geometries and ionic radius (59). Thus, the doping by $\text{Pu}(\text{IV})$ is only possible by allowing it to reside in the void spaces between the neighboring double borate chains (Figure 2b). As a consequence of $\text{Pu}(\text{IV})$ entering the structure, some of the K^+ cations are lost in order to maintain charge-balance, which results in the 3.2% defects on the K sites.

Table 1. Crystallographic information for $\text{K}[\text{B}_5\text{O}_7(\text{OH})_2]\cdot\text{H}_2\text{O}$, $\text{K}[\text{B}_5\text{O}_7(\text{OH})_2]\cdot\text{H}_2\text{O}:\text{Pu}^{4+}$, and larderellite ($\text{NH}_4[\text{B}_5\text{O}_7(\text{OH})_2]\cdot\text{H}_2\text{O}$).

Sample	$\text{K}[\text{B}_5\text{O}_7(\text{OH})_2]\cdot\text{H}_2\text{O}$	$\text{K}[\text{B}_5\text{O}_7(\text{OH})_2]\cdot\text{H}_2\text{O}:\text{Pu}^{4+}$	Larderellite
Color	Colorless	Yellow	Colorless
Space group	$P 2_1/c$	$P 2_1/c$	$P 2_1/c$
a (Å)	9.4824(8)	9.4619(12)	9.47(1)
b (Å)	7.5180(6)	7.4691(10)	7.63(1)

c (Å)	11.4154(6)	11.3740(15)	11.65(1)
α (deg)	90	90	90
β (deg)	97.277(3)	97.412(1)	97.08(25)
γ (deg)	90	90	90
V (Å ³)	807.2(1)	797.1(2)	835.37
Reference	Zhang et al.(57)	This work	Merlino et al.(58)

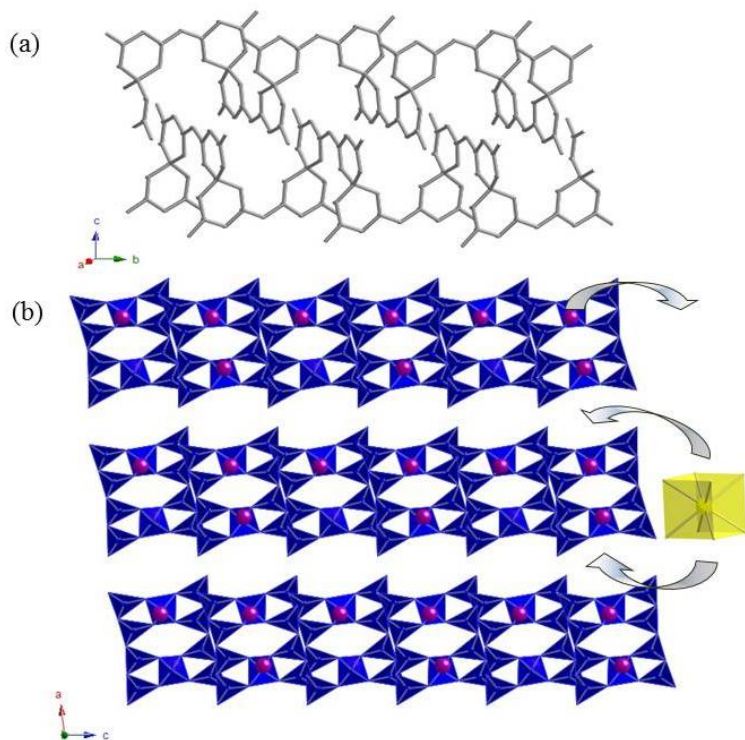


Figure 2. (a) Skeletal structure of double helical one-dimensional borate chains in $K[B_5O_7(OH)_2] \cdot H_2O$. (b) Polyhedral representation of the incorporation mechanism of Pu(IV) into crystals of $K[B_5O_7(OH)_2] \cdot H_2O$. Potassium atoms are shown in purple, borate units (both BO_3 triangles and BO_4 tetrahedra) are shown in blue, and plutonium are shown as yellow cubic polyhedron.

LA-ICP-MS studies. Figure 3 demonstrates a typical time-resolved spectrum (i.e., ion signal measured in counts per second (cps) vs. time (seconds)) for a LA-ICP-MS analysis of a single $K[B_5O_7(OH)_2] \cdot H_2O : Pu^{4+}$ crystal in medium mass resolution mode. It is evident from Figure 3 that ^{242}Pu is incorporated into the crystal (and not solely onto the crystal's surface) since its ion signal measured during the lasering interval is concomitant with those recorded for ^{11}B and ^{39}K , and importantly does not

decrease rapidly with time; the latter feature is consistent for atoms incorporated solely within the surface of the crystal (~first micron of depth). Moreover, repeated analysis (n=9) by LA-ICP-MS of individual $\text{K}[\text{B}_5\text{O}_7(\text{OH})_2] \cdot \text{H}_2\text{O}:\text{Pu}^{4+}$ crystals yielded an average, calculated K:Pu ‘mass’ ratio of 3.37 ± 0.7 . However, a more accurate assessment of the K:Pu ratio should take into account the lower ionization efficiency or lower ‘ion yield’ (ion signal – counts per second/concentration unit) of K versus that for Pu in a plasma environment. In general, the ‘ion yield’ for elements analyzed by an ICP-MS instrument is mass dependent, with ‘heavier’ elements ($>80 \text{ amu}^{-1}$) recording higher values compared to those for lighter elements. The differential ion yield for K versus Pu was assessed in medium mass resolution via the measurement of 4 solutions each containing 1:1 mass ratio of K:U at variable concentrations (~10 to 50 ppb). For ease of sample preparation, uranium was used as a valid proxy for Pu given their similar atomic masses. The average, measured K:U mass ratio obtained for the solutions was 1:3.12. Hence, this result when applied to the laser ablation values yields an average ‘normalized’ K:Pu mass ratio of ~10.5:1, and a corresponding atomic ratio for K:Pu of ~65:1 for the $\text{K}[\text{B}_5\text{O}_7(\text{OH})_2] \cdot \text{H}_2\text{O}:\text{Pu}^{4+}$ crystals.

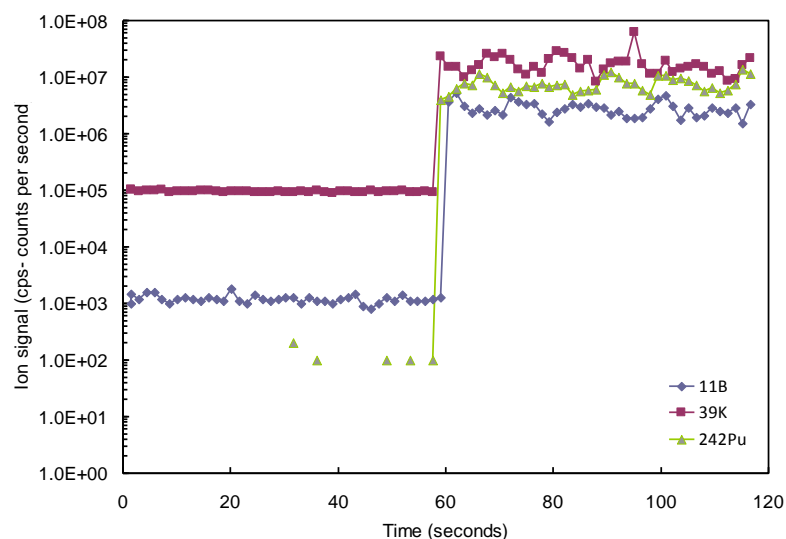


Figure 3. Illustration of a typical time-resolved spectrum (ion signal vs. time) for a LA-ICP-MS analysis of a single $\text{K}[\text{B}_5\text{O}_7(\text{OH})_2] \cdot \text{H}_2\text{O}:\text{Pu}^{4+}$ crystal. Time interval between 0 and ~60 seconds

represents background measurement, whereas subsequent interval represents measurement of ion signals after the start of lasering.

UV-vis-NIR absorption spectroscopy. By possessing complicated f electron configurations, both Pu(IV) and Pu(III) are known to produce a series of weak, Laporte-forbidden f-f transitions in the vis-NIR region in both solution and the solid state (60-61). In solution, the spectrum of Pu(IV) consists of characteristic transitions such as the peaks near 477, 660, 800, 1080 nm (60). For Pu(III), the most important transition that can be used for distinguishing from Pu(IV) is at 920 nm (60). The UV-vis-NIR absorption spectra taken from both freshly-made and one-day old crystals of $\text{K}[\text{B}_5\text{O}_7(\text{OH})_2] \cdot \text{H}_2\text{O}:\text{Pu}^{4+}$ are shown in the Figure 4. It is found that the freshly-made crystals contain dominantly Pu(IV), whereas a very small amount of Pu(III) is also present based on the weak peak at 926 nm. In the spectrum of one-day old crystals, the 926 peak disappears, which indicates that the tiny amount of remaining Pu(III) incorporated into the crystals is rapidly oxidized by ambient O_2 in the air. Nevertheless, the results indicate that both Pu(III) and Pu(IV) are capable of entering the structure of $\text{K}[\text{B}_5\text{O}_7(\text{OH})_2] \cdot \text{H}_2\text{O}$. It should be noted that the incorporation of Pu(III) into $\text{K}[\text{B}_5\text{O}_7(\text{OH})_2] \cdot \text{H}_2\text{O}$ still does not prevent the oxidation of Pu(III). This oxidation contrasts sharply with the fact that many Pu(III) compounds are not air-sensitive (46,62). Apparently, Pu(III) can be further stabilized by the lattice energy in most Pu(III) compounds while the lattice energy is lacking for Pu(III) in crystals of $\text{K}[\text{B}_5\text{O}_7(\text{OH})_2] \cdot \text{H}_2\text{O}$ since plutonium atoms are highly disordered in the void space.

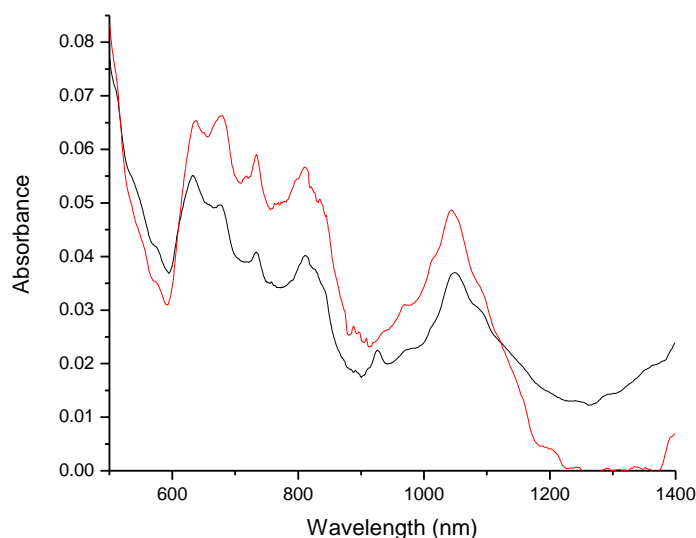


Figure 4. UV-vis-NIR absorption spectra taken from both freshly-made (black) and one-day old (red) crystals of $\text{K}[\text{B}_5\text{O}_7(\text{OH})_2] \cdot \text{H}_2\text{O}:\text{Pu}^{4+}$.

XANES and EXAFS studies. The XANES data shown in Figure 5 are clearly consistent with a Pu(IV) state for the $\text{K}[\text{B}_5\text{O}_7(\text{OH})_2] \cdot \text{H}_2\text{O}:\text{Pu}^{4+}$ sample, as indicated by the consistent position of the white line when compared to data from PuO_2 . Moreover, the first EXAFS oscillation (peak at ~ 18100 eV) is practically identical to that of PuO_2 . The increased peak height of the data indicates differences in the long-range structure, for instance, due to particle or cluster size, which tends to increase the amplitude of the white line for smaller clusters (J. Rothe, C. Walther, M. A. Denecke, T. Fanghanel, XAFS and LIBD investigation of the formation and structure of colloidal Pu(IV) hydrolysis products. *Inorganic Chemistry* 43, 4708-4718 (2004)). Some of this difference could be due to the difference in the measurement temperatures between the borate and the PuO_2 sample.

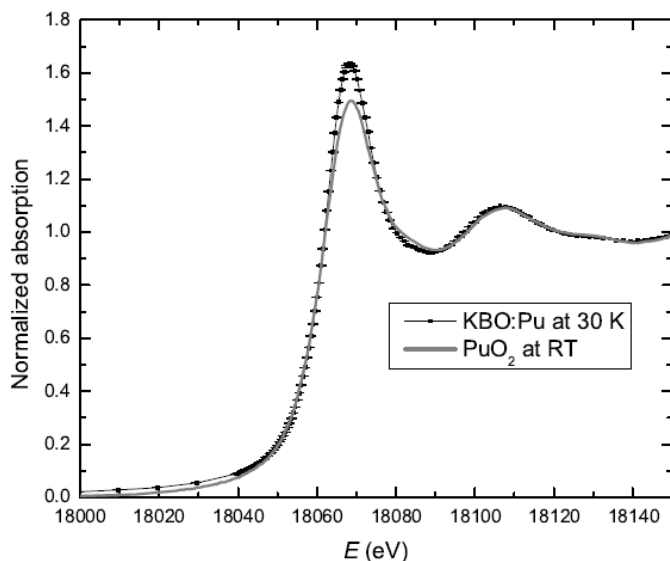


Figure 5. Pu L_{III} -edge XANES of $K[B_5O_7(OH)_2] \cdot H_2O:Pu^{4+}$ at 30 K, together with that of PuO_2 collected at room temperature. Data in this and Figure 6 are displayed with error bars estimated by collecting several scans.

The EXAFS data in Figure 6 are also quite similar to that expected from PuO_2 (not shown in the figure), although the Pu-Pu peak at ~ 3.7 Å in the spectra (corresponding to a Pu-Pu distance of about 3.8 Å) is actually less than half the expected amplitude. The fit results listed in Table 2 clearly indicate the similarity between the measured local structure and that of PuO_2 , as the number of Pu-Pu neighbors is 3.9 ± 0.9 , as opposed to the 12 Pu-Pu neighbors in PuO_2 , the measured Pu-O bond length of 2.325 ± 0.8 Å is typical for a Pu(IV) compound (62), and the amplitude reduction factor S_0^2 is reasonable given an oxygen coordination of 8 around the Pu atoms. It should be noted, however, that the estimated error in S_0^2 allows for 9 Pu-O nearest-neighbors.

These data are not compatible with a significant number of Pu atoms occupying the K position in the structure of $K[B_5O_7(OH)_2] \cdot H_2O$. In that structure, the K-O near neighbor shell has 10 neighbors with bond lengths between 2.76 and 3.22 Å, which would generate an EXAFS peak approximately 15% of the amplitude at centered about 0.4 Å further in the Fourier transform of Figure 6. Even if one allows for a local rearrangement of O around Pu when Pu occupies a K site, one would not expect a Pu-Pu pair at 3.8 Å in this structure, where the K-K nearest distance is about 5.0 Å with only two neighbors. These

data are therefore more consistent with PuO₂ clusters, rather than a random distribution of Pu on K positions within the K[B₅O₇(OH)₂]·H₂O structure.

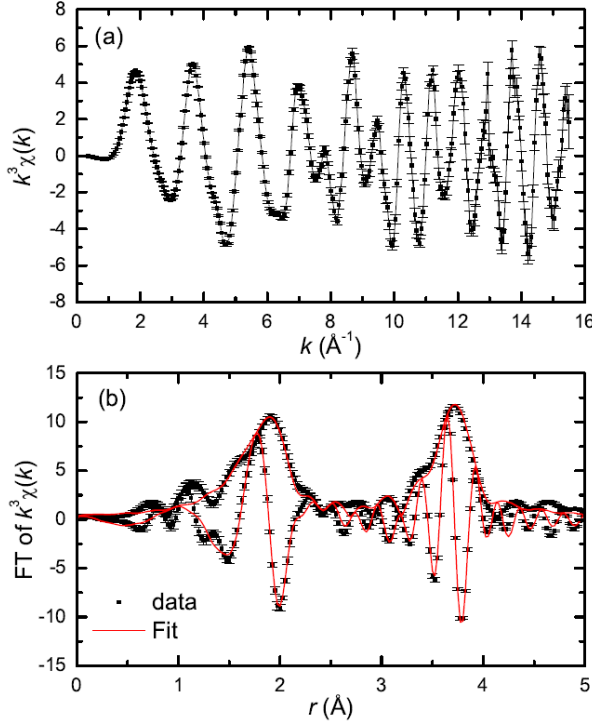


Figure 6. Pu L_{III} -edge EXAFS data from K[B₅O₇(OH)₂]·H₂O:Pu⁴⁺ at 30 K in both (a) k -space and (b) r -space. The Fourier transform (FT) in (b) shows the amplitude (outer envelope) and the real part (modulating line) of the transform, and is taken between 2.5-15.0 Å⁻¹, Gaussian narrowed by 0.3 Å⁻¹. The fit shown in (b) is between 1.8 and 3.9 Å. Fit results are summarized in Table 2.

Table 2. Fit results for Pu L_{III} -edge EXAFS data on K[B₅O₇(OH)₂]·H₂O:Pu⁴⁺ at T = 30 K. Fit range is between 1.8 and 3.9 Å. The k^3 -weighted data are transformed between 2.5-15.0 Å⁻¹ and are Gaussian narrowed by 0.3 Å⁻¹. The degree of freedom of the fit is estimated to be 11.7 (63). Error estimates use a Monte Carlo method (64). The amplitude reduction factor for these fits is determined to be $S_0^2 = 1.14 \pm 0.14$ and the edge shift is $\Delta E_0 = -11.0 \pm 0.9$ eV.

	N	$\sigma^2(\text{\AA}^2)$	$R(\text{\AA})$
Pu-O	8	0.010(1)	2.325(8)

Pu-Pu	3.9(9)	0.0027(5)	3.808(4)
ΔE_0		-11.0(9)	
S_0^2		1.14(14)	
$R(\%)$		12.7	

Implications for the migration of radionuclides at repositories and designing of novel waste forms. It is well known that the release of radionuclides at repositories is retarded by the incorporation of radionuclides into natural materials. However, predictions of actinide incorporation based solely on the old lattice substitution mechanism now seem to be very limited. With our observation of a new incorporation mechanism occurring in $\text{K}[\text{B}_5\text{O}_7(\text{OH})_2]\cdot\text{H}_2\text{O}:\text{Pu}^{4+}$, many natural materials that lack suitable sites for lattice substitution but that possess void spaces of suitable dimensions may also show the capacity for trapping certain radionuclides. Furthermore, studies focused on the incorporation of actinides into borate minerals are scarce. This study is pertinent and significant for the Waste Isolation Pilot Plant (WIPP) located at the Salado formation near Carlsbad, NM, where the concentration of borates, predominately in forms of H_3BO_3 , $\text{B}(\text{OH})_4^-$, and $\text{B}_4\text{O}_7^{2-}$, attains concentrations as high as 166 ppm in intergranular brines (65). Borate minerals are known to have a very complicated and rich structural chemistry, and countless structural topologies have been observed in the borate mineral family (66-67). A variety of borate minerals including larderellite (natural analogue of $\text{K}[\text{B}_5\text{O}_7(\text{OH})_2]\cdot\text{H}_2\text{O}$) are expected to form in the WIPP that can provide a series of structures containing void space with a wide range of dimensions. These void spaces could trap actinides, which would slow down their migration.

However, simple actinide capture is not the sole, primary message of this work. Our study clearly indicates that $\text{K}[\text{B}_5\text{O}_7(\text{OH})_2]\cdot\text{H}_2\text{O}:\text{Pu}^{4+}$ is a material capable of trapping and stabilizing actinides without lattice substitution. From our observations, Pu(IV) is not released when the crystals of $\text{K}[\text{B}_5\text{O}_7(\text{OH})_2]\cdot\text{H}_2\text{O}:\text{Pu}^{4+}$ are refluxed in boiling water. Therefore, this novel incorporation mechanism should be considered for new waste form designs in addition to the current choices in debate such as perovskite, pyrochlore, zirconolite, zircon, monazite, and garnet, which are all based on the mechanism

of lattice substitution (4-6). For example, zeolites contain numerous types of void spaces that can be used for selectively trapping actinides of certain size and charge (68-69). In the near future, we will investigate this hypothesis along with other low-dimensional borate materials.

Acknowledgments

We are grateful for support provided by the U.S. Department of Energy, Subsurface Biogeochemical Research Program. Work at Lawrence Berkeley National Laboratory was supported by the Director, OS, OBES, of the U.S. DOE under Contract No. DE-AC02-05CH11231.

Supporting Information. EDS result and X-ray file (CIF) for $\text{K}[\text{B}_5\text{O}_7(\text{OH})_2]\cdot\text{H}_2\text{O}:\text{Pu}^{4+}$. This material is available free of charge at <http://pubs.acs.org>.

Literature Cited

- (1) Novikov, A. P.; Kalmykov, S. N.; Utsunomiya, S.; Ewing, R. C.; Horreard, F.; Merkulov, A.; Clark, S. B.; Tkachev, V. V.; Myasoedov, B. F. Colloid transport of plutonium in the Far-Field of the Mayak Production Association, Russia. *Science* **2006**, *314*, 638-641.
- (2) Pockley, P. Clean-up strategy at Australian nuclear site called into question. *Nature* **2000**, *404*, 797-797.
- (3) Dai, M.; Kelly, J. M.; Buesseler, K. O. Sources and migration of plutonium in groundwater at the Savannah River Site. *Environ. Sci. Technol.* **2002**, *36*, 3690-3699.
- (4) Lumpkin, G. R. Ceramic waste forms for actinides. *Elements* **2006**, *2*, 365-372.

- (5) Ewing, R. C. Nuclear waste forms for actinides. *Proc. Natl. Acad. Sci. USA* **1999**, *96*, 3432-3439.
- (6) Donald, I. W.; Metcalfe, B. L.; Taylor, R. N. J. The immobilization of high level radioactive wastes using ceramics and glasses. *J. Mat. Sci.* **1997**, *32*, 5851-5887.
- (7) Sturchio, N. C.; Antonio, M. R.; Soderholm, L.; Sutton, S. R.; Brannon, J. C. Tetravalent uranium in calcite. *Science* **1998**, *281*, 971-973.
- (8) Kelly, S. D.; Troy Rasbury, E.; Chattopadhyay, S.; Jeremy Kropf, A.; Kemner, K. M. Evidence of a stable uranyl site in ancient organic-rich calcite. *Environ. Sci. Technol.* **2006**, *40*, 2262-2268.
- (9) Kelly, S. D.; Newville, M. G.; Cheng, L.; Kemner, K. M.; Sutton, S. R.; Fenter, P.; Sturchio, N. C.; Spotl, C. Uranyl incorporation in natural calcite. *Environ. Sci. Technol.* **2003**, *37*, 1284-1287.
- (10) Wang, Z.; Zachara, J. M.; Mckinley, J. P.; Smith, S. C. Cryogenic laser induced U(VI) fluorescence studies of a U(VI) substituted natural calcite: implications to U(VI) speciation in contaminated Hanford sediments. *Environ. Sci. Technol.* **2005**, *39*, 2561-2659.
- (11) Heberling, F.; Denecke, M. A.; Bosbach, D. Neptunium(V) coprecipitation with calcite. *Environ. Sci. Technol.* **2008**, *42*, 471-476.
- (12) Reeder, R. J.; Elzinga, E. J.; Drew Tait, C.; Rector, K. D.; Donohoe, R. J.; Morris, D. E. Site-specific incorporation of uranyl carbonate species at the calcite surface. *Geochim. Cosmochim. Acta* **2004**, *68*, 4799-4808.
- (13) Valle-Fuentes, F.-J.; Garcia-Guinea, J.; Cremades, A.; Correcher, V.; Sanchez-Moral, S.; Gonzalez-Martin, R.; Sanchez-Munoz, L.; Lopez-Arce, P. Low-magnesium uranium-calcite with high degree of crystallinity and gigantic luminescence emission. *Appl. Radiat. Isotopes* **2007**, *65*, 147-154.
- (14) Arai, Y.; Marcus, M. A.; Tamura, N.; Davis, J. A.; Zachara, J. M. Spectroscopic evidence for uranium bearing precipitates in Vadose Zone sediments at the Hanford 300-area. *Environ. Sci. Technol.* **2007**, *41*, 4633-4639.

- (15) Marques Fernandes, M.; Stumpf, T.; Rabung, T.; Bosbach, D.; Fanghanel, Th. Incorporation of trivalent actinides into calcite: A time resolved laser fluorescence spectroscopy (TRLFS) study. *Geochim. Cosmochim. Acta* **2008**, 72, 464-474.
- (16) Ewing, R. C.; Lutze, W.; Weber, W. J. Zircon: a host-phase for the disposal of weapons plutonium. *J. Mat. Res.* **1995**, 10, 243-246.
- (17) Meldrum, A.; Boatner, L. A.; Ewing, R. C. Displacive radiation effects in the monazite- and zircon-structure orthophosphates. *Phys. Rev. B* **1997**, 56, 13805-13814.
- (18) Deschanel, X.; Picot, V.; Glorieux, B.; Jorion, F.; Peugeot, S.; Roudil, D.; Jegou, C.; Broudic, V.; Cachia, J. N.; Advocat, T.; Den Auwer, C.; Fillet, C.; Coutures, J. P.; Hennig, C.; Scheinost, A. Plutonium incorporation in phosphate and titanate ceramics for minor actinide containment. *J. Nucl. Mat.* **2006**, 352, 223-240.
- (19) Vance, E. R.; Ball, C. J.; Day, R. A.; Smith, K. L.; Blackford, M. G.; Begg, B. D.; Angel, P. J. Actinide and rare earth incorporation into zirconolite. *J. Alloy Compd.* **1994**, 213/214, 406-409.
- (20) Clinard, F. W. Jr; Rohr, D. L.; Roof, R. B. Structural damage in a self-irradiated zirconolite-based ceramic. *Nucl. Instrum. Meth. Phys. Res. B* **1984**, 1, 581-586.
- (21) Weber, W. J.; Wald, J. W.; Matzke, H. Effects of self-radiation damage in Cm-doped $\text{Gd}_2\text{Ti}_2\text{O}_7$ and $\text{CaZrTi}_2\text{O}_7$. *J. Nucl. Mat.* **1986**, 138, 196-209.
- (22) Begg, B. D.; Vance, E. R.; Conradson, S. D. The incorporation of plutonium and neptunium in zirconolite and perovskite. *J. Alloy Compd.* **1998**, 271-273, 221-226.
- (23) Nastren, C.; Jardin, R.; Somers, J.; Walter, M.; Brendebach, B. Actinide incorporation in a zirconia based pyrochlore $(\text{Nd}_{1.8}\text{An}_{0.2})\text{Zr}_2\text{O}_{7+x}$ (An = Th, U, Np, Pu, Am). *J. Solid State Chem.* **2009**, 182, 1-7.
- (24) Ewing R. C.; Weber, W. J.; Lian, J. Nuclear waste disposal-pyrochlore ($\text{A}_2\text{B}_2\text{O}_7$): Nuclear waste form for the immobilization of plutonium and “minor” actinides. *J. Appl. Phys.* **2004**, 95, 5949-5971.

- (25) Strachan, D. M.; Scheele, R. D.; Buck, E. C.; Icenhower, J. P.; Kozelisky, A. E.; Sell, R. L.; Elovich, R. J.; Buchmiller, W. C. Radiation damage effects in candidate titanates for Pu disposition: Pyrochlore. *J. Nucl. Mat.* **2005**, *345*, 109-135.
- (26) Douglas Farr, J.; Neu, M. P.; Schulze, R. K.; Honeyman, B. D. Plutonium uptake by brucite and hydroxylated periclase. *J. Alloy Compd.* **2007**, *444-445*, 553-539.
- (27) Meis, C.; Gale, J. D.; Boyer, L.; Carpena, J.; Gosset, D. Theoretical study of Pu and Cs incorporation in a mono-silicate neodymium fluoroapatite $\text{Ca}_9\text{Nd}(\text{SiO}_4)(\text{PO}_4)_5\text{F}_2$. *J. Phys. Chem. A* **2000**, *104*, 5380-5387.
- (28) Yamazaki, S.; Yamashita, T.; Matsui, T.; Nagasaki, T. Thermal expansion and solubility limits of plutonium-doped lanthanum zirconates. *J. Nucl. Mat.* **2001**, *294*, 183-187.
- (29) Vance, E. R.; Ball, C. J.; Begg, B. D.; Carter, M. L.; Arthur Day, R.; Thorogood, G. J. Pu, U, and Hf incorporation in Gd silicate apatite. *J. Am. Ceram. Soc.* **2003**, *86*, 1223-1225.
- (30) Holiday, K.; Hartmann, T.; Mulcahy, S. R.; Czerwinski, K. Synthesis and characterization of zirconia-magnesia inert matrix fuel: plutonium studies. *J. Nucl. Mat.* **2010**, *402*, 81-86.
- (31) Burns, P. C.; Finch, R. J.; Hawthorne, F. C.; Miller, M. L.; Ewing, R. C. The crystal structure of ianthinite, $[\text{U}_2^{4+}(\text{UO}_2)_4\text{O}_6(\text{OH})_4(\text{H}_2\text{O})_4](\text{H}_2\text{O})_5$: a possible phase for Pu^{4+} incorporation during the oxidation of spent nuclear fuel. *J. Nucl. Mat.* **1997**, *249*, 199-206.
- (32) Burns, P. C.; Ewing, R. C.; Miller, M. L. Incorporation mechanisms of actinide elements into the structures of U^{6+} phases formed during the oxidation of spent nuclear fuel. *J. Nucl. Mat.* **1997**, *245*, 1-9.
- (33) Dacheux, N.; Grandjean, S.; Rousselle, J.; Clavier, N. Hydrothermal method of preparation of actinide(IV) phosphate hydrogenphosphate hydrates and study of their conversion into actinide(IV) phosphate diphosphate solid solutions. *Inorg. Chem.* **2007**, *46*, 10390-10399.

- (34) Krupa, J. C.; Carnall, W. T. Electronic structure of U^{4+} , Np^{4+} , and Pu^{4+} doped into $ThSiO_4$ single crystal. *J. Chem. Phys.* **1993**, *99*, 8577-8584.
- (35) Wu, S.; Chen, F.; Simonetti, A.; Albrecht-Schmitt, T. E. Incorporation of neptunium(V) and iodate into a uranyl phosphate: implications for mitigating the release of ^{237}Np and ^{129}I in repositories. *Environ. Sci. Technol.* **2010**, *44*, 3192-3196.
- (36) Wang, S.; Alekseev, E. V.; Diwu, J.; Casey, W. H.; Phillips, B. L.; Depmeier, W.; Albrecht-Schmitt, T. E. NDTB-1: A supertetrahedral cationic framework that removes TcO_4^- from solution. *Angewandte Chemie, Int. Ed.* **2010**, *49*, 1057-1060.
- (37) Yu, P.; Wang, S.; Alekseev, E. V.; Depmeier, W.; Albrecht-Schmitt, T. E.; Phillips, B.; Casey, W. Technetium-99 MAS NMR spectroscopy of a cationic framework material that traps TcO_4^- ions. *Angew. Chem. Int. Ed.* **2010**, *49*, 5975-5977.
- (38) Wang, S.; Alekseev, E. V.; Ling, J.; Liu, G.; Depmeier, W.; Albrecht-Schmitt, T. E. Polarity and chirality in uranyl borates: insights into understanding the vitrification of nuclear waste and the development of nonlinear optical materials. *Chem. Mater.* **2010**, *22*, 2155-2163.
- (39) Wang, S.; Alekseev, E. V.; Stritzinger, J. T.; Depmeier, W.; Albrecht-Schmitt, T. E. How are centrosymmetric and noncentrosymmetric structures achieved in uranyl borates? *Inorg. Chem.* **2010**, *49*, 2948-2953.
- (40) Wang, S.; Alekseev, E. V.; Stritzinger, J. T.; Depmeier, W.; Albrecht-Schmitt, T. E. Crystal chemistry of the potassium and rubidium uranyl borate families derived from boric acid fluxes. *Inorg. Chem.* **2010**, *49*, 6690-6696.
- (41) Wang, S.; Alekseev, E. V.; Stritzinger, J. T.; Liu, G.; Depmeier, W.; Albrecht-Schmitt, T. E. Structure-property relationships in lithium, silver, and cesium uranyl borates. *Chem. Mater.* **2010**, *22*, 5983-5991.

- (42) Wang, S.; Alekseev, E. V.; Ling, J.; Skanthakumar, S.; Soderholm, L.; Depmeier, W.; Albrecht-Schmitt, T. E. Neptunium diverges sharply from uranium and plutonium in crystalline borate matrixes: insights into the complex behavior of the early actinides relevant to nuclear waste storage. *Angew. Chem. Int. Ed.* **2010**, *49*, 1263-1266.
- (43) Wang, S.; Alekseev, E. V.; Depmeier, W.; Albrecht-Schmitt, T. E. Further insights into intermediate- and mixed-valency in neptunium oxoanion compounds: structure and absorption spectroscopy of $K_2[(NpO_2)_3B_{10}O_{16}(OH)_2(NO_3)_2]$. *Chem. Com.* **2010**, *46*, 3955-3957.
- (44) Wang, S.; Alekseev, E. V.; Miller, H. M.; Depmeier, W.; Albrecht-Schmitt, T. E. Boronic acid flux synthesis and crystal growth of uranium and neptunium boronates and borates: a low-temperature route to the first neptunium(V) borate. *Inorg. Chem.* **2010**, *49*, 9755-9757.
- (45) Wang, S.; Villa, E. M.; Diwu, J.; Alekseev, E. V.; Depmeier, W.; Albrecht-Schmitt, T. E. Role of anions and reaction conditions in the preparation of uranium(VI), neptunium(VI), and plutonium(VI) borates. *Inorg. Chem.* **2011**, *50*, 2527-2533.
- (46) Wang, S.; Alekseev, E. V.; Depmeier, W.; Albrecht-Schmitt, T. E. Surprising coordination for plutonium in the first plutonium(III) borate. *Inorg. Chem.* **2011**, *50*, 2079-2081.
- (47) Wang, S.; Alekseev, E. V.; Diwu, J.; Miller, H. M.; Oliver, A.; Liu, G.; Depmeier, W.; Albrecht-Schmitt, T. E. Functionalization of borate networks by the incorporation of fluoride: syntheses, crystal structures, and nonlinear optical properties of novel actinide fluoroborates. *Chem. Mater.* **2011**, *23*, 2931-2939.
- (48) Chu, S. N. G.; Logan, R. A.; Geva, M.; Ha, N. T.; Karlicek, R. F. Substitutional, interstitial, and neutral zinc incorporation into InP grown by atmospheric pressure metalorganic vapor phase epitaxy. *J. Appl. Phys.* **1996**, *80*, 3221-3227.

- (49) Lehmann, G. Interstitial incorporation of di- and trivalent cobalt in quartz. *J. Phys. Chem. Solids* **1969**, *30*, 395-399.
- (50) Wu, S.; Wang, S.; Simonetti, A.; Chen, F.; Albrecht-Schmitt, T. E. Incorporation of iodate into uranyl borates and its implication for the immobilization of ^{129}I in nuclear waste repositories. *Radiochim. Acta* **2011**, *99*, 1–7.
- (51) Sheldrick, G. M. *SADABS* 2001, Program for absorption correction using SMART CCD based on the method of Blessing: Blessing, R. H. *Acta Cryst.* **1995**, *A51*, 33-38.
- (52) Simonetti, A.; Heaman, L. M.; Chacko, T.; Banerjee, N. R. In-situ petrographic thin section U-Pb dating of zircon, monazite, and titanite using laser ablation-MC-ICP-MS. *Int. J. Mass Spectrom.* **2006**, *253*, 87-97.
- (53) Simonetti, A.; Heaman, L. M.; Chacko, T. Use of discrete-dynode secondary electron multipliers with Faradays – A ‘reduced volume’ approach for in-situ U-Pb dating of accessory minerals within petrographic thin section by LA-MC-ICP-MS, in *2008 V.M. Goldschmidt Laser Ablation Short Course 40*; Sylvester, P., Eds.; Vancouver, BC 2008; pp 241-264.
- (54) Booth, C. H.; Bridges, F. Improved self-absorption correction for fluorescence measurements of extended X-ray absorption fine-structure. *Phys. Scripta* **2005**, *T115*, 202-204.
- (55) Hayes, T. M.; Boyce, J. B. Extended X-ray absorption fine structure. *Solid State Physics Academic*, New York, 1982, vol. 37, pp 173-351.
- (56) Li, G. G.; Bridges, F.; Booth, C. H. X-ray-absorption fine-structure standards: a comparison of experiment and theory. *Phys. Rev. B* **1995**, *52*, 6332-6348.
- (57) Zhang, H.-X.; Zhang, J.; Zheng, S.-T.; Yang, G.-Y. Two new potassium borates, $\text{K}_4\text{B}_{10}\text{O}_{15}(\text{OH})_4$ with stepped chain and $\text{KB}_5\text{O}_7(\text{OH})_2 \cdot \text{H}_2\text{O}$ with double helical chain. *Cryst. Growth Des.* **2005**, *5*, 157-161.

- (58) Merlino, S.; Sartori, F. The crystal structure of lardellite, $\text{NH}_4\text{B}_5\text{O}_7(\text{OH})_2 \cdot \text{H}_2\text{O}$. *Acta Cryst.* **1969**, B25, 2264-2270.
- (59) Shannon, R. D. Revised effective ionic radii and systematic studies of interatomic distances in halides and chalcogenides. *Acta Cryst.* **1976**, A32, 751-767.
- (60) Lee, M. H.; Park, Y. J.; Kim, W. H. Absorption spectroscopic properties for Pu(III, IV and VI) in nitric and hydrochloric acid media. *J. Radioanalytical Nucl. Chem.* **2007**, 273, 375-382.
- (61) Liu, G.; Beitz, J. V. *Spectra and Electronic Structures of Free Actinide Atoms*, in *The Chemistry of the Actinide and Transactinide Elements*, ed. Morss, L. R.; Edelstein, N. M.; Fuger, J. Springer, The Netherlands, 2006, vol. 4, chapter 16, pp. 2013-2111.
- (62) Clark, D. L.; Hecker, S. S.; Jarvinen, G. D.; Neu, M. P. *Plutonium*, in *The Chemistry of the Actinide and Transactinide Elements*, ed. Morss, L. R.; Edelstein, N. M.; Fuger, J. Springer, The Netherlands, 2006, vol. 2, chapter 7, pp. 813-1264.
- (63) Stern, E. A.; Livins, P.; Zhang, Z. Thermal vibration and melting from a local perspective. *Phys. Rev. B* **1991**, 43, 8850-8860.
- (64) Hu, Y.-J.; Booth, C. H. Predetermining acceptable noise limits of EXAFS spectra in the limit of stochastic noise. *J. Phys. Conf. Ser.* **2009**, 190, 012028.
- (65) Snider, A. C. *Verification of the Definition of Generic Weep Brine and the Development of a Recipe for This Brine*. ERMS 527505.
- (66) Burns, P. C.; Grice, J. D.; Hawthorne, F. C. Borate minerals: I. Polyhedral clusters and fundamental building blocks. *Can. Mineral.* **1995**, 33, 1131-1151.
- (67) Grice, J. D.; Burns, P. C.; Hawthorne, F. C. Borate minerals: II. A hierarchy of structures based upon the borate fundamental building block. *Can. Mineral.* **1999**, 37, 731-762.

(68) Suib, S. L. Zeolitic and layered materials. *Chem. Rev.* **1993**, 93, 803-826.

(69) Smith, Joseph V. Topochemistry of zeolites and related materials. 1. Topology and geometry. *Chem. Rev.* **1988**, 88, 149-182.

Brief: The interstitial incorporation of plutonium into $\text{K}[\text{B}_5\text{O}_7(\text{OH})_2] \cdot \text{H}_2\text{O}$ provides a novel mechanism for the incorporation of actinides into natural materials and new waste form design.

DISCLAIMER

This document was prepared as an account of work sponsored by the United States Government. While this document is believed to contain correct information, neither the United States Government nor any agency thereof, nor the Regents of the University of California, nor any of their employees, makes any warranty, express or implied, or assumes any legal responsibility for the accuracy, completeness, or usefulness of any information, apparatus, product, or process disclosed, or represents that its use would not infringe privately owned rights. Reference herein to any specific commercial product, process, or service by its trade name, trademark, manufacturer, or otherwise, does not necessarily constitute or imply its endorsement, recommendation, or favoring by the United States Government or any agency thereof, or the Regents of the University of California. The views and opinions of authors expressed herein do not necessarily state or reflect those of the United States Government or any agency thereof or the Regents of the University of California.